

1 **SARS-CoV-2 disinfection in aqueous solution** 2 **by UV₂₂₂ from a krypton chlorine excilamp** 3 4

5 **AUTHORS**

6 Richard T. Robinson^{1,2}, Najmus Mahfooz¹, Oscar Rosas-Mejia¹, Yijing Liu³, Natalie M.
7 Hull^{3,4*}
8

9 **AFFILIATIONS**

- 10 1. Department of Microbial Infection and Immunity, The Ohio State University,
11 Columbus, OH, USA
12 2. Infectious Diseases Institute, The Ohio State University, Columbus, OH, USA
13 3. Department of Civil, Environmental, and Geodetic Engineering, The Ohio State
14 University, Columbus, OH, USA
15 4. Sustainability Institute, The Ohio State University, Columbus, OH, USA
16 * Corresponding author: Natalie Hull, hull.305@osu.edu, 2070 Neil Ave, Hitchcock
17 417C, Columbus, OH,43210
18

19 **KEYWORDS**

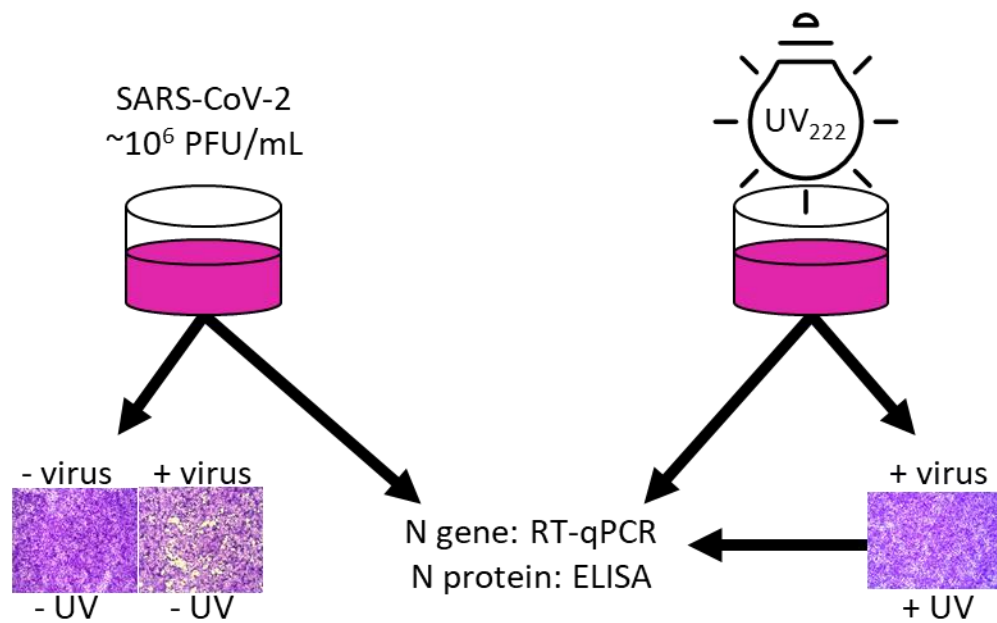
20 COVID-19, SARS-CoV-2, UV Disinfection, ultraviolet light, water treatment, coronavirus,
21 qPCR, plaque assay, infectivity, nucleic acid damage, protein damage, ELISA, RNA
22
23

24 **ABSTRACT**

25 There is an urgent need for evidence-based development and implementation of
26 engineering controls to reduce transmission of SARS-CoV-2, the etiological agent of
27 COVID-19. Ultraviolet (UV) light can inactivate coronaviruses, but the practicality of UV
28 light as an engineering control in public spaces is limited by the hazardous nature of
29 conventional UV lamps, which are Mercury (Hg)-based and emit a peak wavelength
30 (254 nm) that penetrates human skin and is carcinogenic. Recent advances in the
31 development and production of Krypton Chlorine (KrCl) excimer lamps hold promise in
32 this regard, as these emit a shorter peak wavelength (222 nm) and are recently being
33 produced to filter out emission above 240 nm. However, the disinfection kinetics of KrCl
34 UV excimer lamps against SARS-CoV-2 are unknown. Here we provide the first dose
35 response report for SARS-CoV-2 exposed to a commercial filtered KrCl excimer light
36 source emitting primarily 222 nm UV light (UV₂₂₂), using multiple assays of SARS-CoV-
37 2 viability. Plaque infectivity assays demonstrate the pseudo-first order rate constant of
38 SARS-CoV-2 reduction of infectivity to host cells to be 0.64 cm²/mJ (R² = 0.95), which
39 equates to a D₉₀ (dose for 1 log₁₀ or 90% inactivation) of 1.6 mJ/cm². Through RT-
40 qPCR assays targeting the nucleocapsid (N) gene with a short (<100 bp) and long
41 (~1000 bp) amplicon in samples immediately after UV₂₂₂ exposure, the reduction of
42 ability to amplify indicated an approximately 10% contribution of N gene damage to
43 disinfection kinetics. Through ELISA assay targeting the N protein in samples
44 immediately after UV₂₂₂ exposure, we found no dose response of the ability to damage
45 the N protein. In both qPCR assays and the ELISA assay of viral outgrowth
46 supernatants collected 3 days after incubation of untreated and UV₂₂₂ treated SARS-
47 CoV-2, molecular damage rate constants were similar, but lower than disinfection rate
48 constants. These data provide quantitative evidence for UV₂₂₂ doses required to
49 disinfect SARS-CoV-2 in aqueous solution that can be used to develop further
50 understanding of disinfection in air, and to inform decisions about implementing UV₂₂₂
51 for preventing transmission of COVID19.

52

53 **ABSTRACT ART / TOC GRAPHIC**



54

55

56

57 INTRODUCTION

58 Severe acute respiratory syndrome coronavirus 2 (SARS-CoV-2) is the etiological agent
59 of Coronavirus Disease 2019 (COVID-19), a recently emerged infectious disease with
60 no cure. SARS-CoV-2 spreads primarily from person to person when mucous
61 membranes (e.g., lungs, eyes) are exposed to airborne viruses that have been emitted
62 by infected individuals in particles of various size^{1,2}. Infection leads to a variable
63 disease course affecting multiple organ systems (respiratory, cardiac, neurological and
64 gastrointestinal); for this reason, the symptoms of COVID19 are variable and include
65 asymptomatic infection, fever, cough, dyspnea, malaise, nausea, ageusia/anosmia,
66 delirium and death. A number of antiviral and host-directed therapies have been or are
67 being explored as COVID19 treatments, including low-dose radiation³, nucleoside
68 analogs (e.g. remdesivir⁴, favipiravir⁵), hydroxychloroquine⁶, interferon beta⁷,
69 convalescent plasma^{8,9}, neutralizing monoclonal antibodies^{10,11}, and anti-inflammatories
70 such as dexamethasone¹², IL6 inhibitors¹³, and JAK/STAT inhibitors¹⁴. Prophylactic
71 vaccines against the SARS-CoV-2 Spike protein have also recently become available¹⁵.
72 These treatments and vaccines are causes for optimism during the current COVID19
73 pandemic, which to date has killed nearly 2 million individuals; however, even after
74 vaccines become widely available, social distancing, face masks and other engineering
75 solutions that limit transmission will continue to be needed in the foreseeable future for
76 this and other emerging infectious diseases¹⁶.

77
78 Ultraviolet (UV) irradiation is an effective means of inactivating a number of respiratory
79 viruses, including human coronavirus OC43 (HCoV-OC43, a cause of the common
80 cold¹⁷) and SARS-CoV (etiological agent of the 2002 SARS epidemic¹⁸⁻²⁰). UV is
81 commonly applied for upper room air disinfection, in HVAC systems, and in free-
82 standing air and surface purifiers. The feasibility of using UV on a widespread and
83 evidence-based level to minimize transmission of SARS-CoV-2, however, is currently
84 limited by two reasons: (1) conventional mercury-based low pressure UV lamps are
85 impractical in many settings as they are hazardous to human health (the 254 nm
86 wavelength emission causes skin cancer²¹ and cataracts²²) and the environment

87 (mercury from breaking fragile quartz lamp bulbs is toxic²³), (2) the UV dose response
88 kinetics needed to inactivate SARS-CoV-2 are unknown. Should these two challenges
89 be overcome, the use of UV to inactivate SARS-CoV-2 in environments with high
90 potential for transmission (e.g. congregate care facilities, convalescent patient homes,
91 hospital waiting rooms, airplane cabins) would be a practical and readily deployed
92 engineering solution to augment current prophylactic measures (social distancing, face
93 masks, vaccines). Due to a surge in interest and application of UV in various public
94 settings, there is an urgent need to understand the dose response kinetics of SARS-
95 CoV-2 to UV radiation to inform decisions which balance the risk to eyes and skin from
96 UV exposure with the risk of infection from virus transmission.

97
98 Here we demonstrate the dose response kinetics of SARS-CoV-2 in liquid after
99 exposure to primarily 222 nm UV light emitted by a krypton-chlorine (KrCl) excimer lamp
100 (excilamp) filtered to reduce transmission of more harmful wavelengths > 240 nm. The
101 lower wavelength emission (222 nm) is neither carcinogenic in human skin models or
102 rodents²⁴, nor causes acute corneal damage in rodents²⁵. Additionally, the 222 nm
103 wavelength emitted by KrCl excilamps is inherently more effective at disinfection²⁶,
104 nucleic acid damage²⁷, and protein damage^{28,29} than 254 nm emitted by low pressure
105 mercury lamps due to greater absorbance of target biomolecules at lower wavelengths.
106 Krypton and chlorine in KrCl excilamps are much less toxic than mercury, and KrCl
107 excilamps have already been shown to be competitive in terms of electrical efficiency
108 with mercury lamps that have many more years of product development and
109 optimization³⁰. Our results demonstrate that when an aqueous solution of pathogenic
110 SARS-CoV-2 is exposed to UV₂₂₂ light emitted by a Kr-Cl excilamp, its infectivity and
111 integrity is attenuated in a UV dose-dependent manner, as measured by culture and
112 molecular assays. These first UV₂₂₂ disinfection dose responses demonstrate the
113 feasibility of UV as an approach to inactivate SARS-CoV-2.

114 **METHODS**

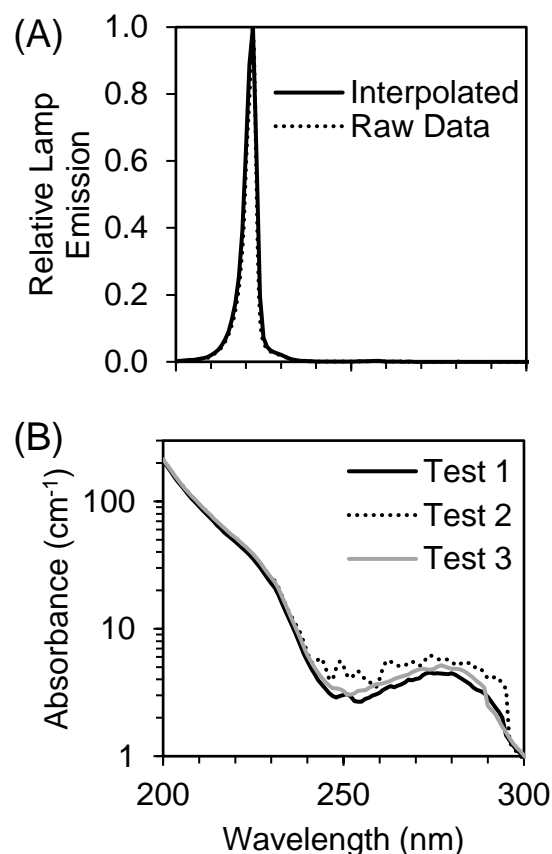
115 **SARS-CoV-2 culture**

116 SARS-CoV-2, Isolate USA-WA1/2020, was obtained from Biodefense and Emerging
117 Infections Research Resources Repository (BEI Resources, Batch # 70034262) and
118 stored and cultured in the Ohio State University Biosafety Level 3 laboratory (IBC
119 Protocol # 2020R00000046). The viral stock used in this study was established by
120 thawing the Batch, diluting it 1:10,000 into incomplete DMEM (Gibco Cat# 11995-065,
121 supplemented with 4.5 g/L D-glucose, 110 mg/L sodium pyruvate), and adding it to
122 T175 flasks of confluent Vero cells (ATCC clone E6) for a one hour incubation period
123 (37°C, 5% CO₂), after which the supernatant was removed and replaced with complete
124 DMEM (cDMEM; DMEM as above plus 4% heat-inactivated fetal bovine serum). These
125 T175 flasks were incubated for 3 days (37°C, 5% CO₂) to propagate infectious virus. At
126 the end of this period, visual inspection of the flasks under a light microscope
127 demonstrated that the nearly all Vero cells were dead. The supernatants in each of the
128 T175 flasks were presumed to contain infectious virus at this point, were carefully
129 transferred and combined into a 50mL conical, centrifuged at low speed to remove cell
130 debris, aliquoted into microcentrifuge tubes, frozen and stored at -80°C. The live virus
131 titer in frozen aliquots was determined to be ~10⁷ plaque forming unit (PFU) per mL
132 using a modified version of plaque assay developed by the Diamond laboratory³¹ and
133 described below.

134 **UV Dose Calculations**

135 The UV₂₂₂ light source (USHIO Care222[®]) is a KrCl excilamp that is optically filtered to
136 reduce emission > 240 nm. The UV source was turned on to warm up for 15 minutes
137 before any irradiance or spectral measurements or irradiations. Standardized
138 procedures were followed for carrying out quasi-collimated beam disinfection studies³²
139 and calculating polychromatic UV doses³³. The emission spectrum of the UV₂₂₂ source
140 was measured using a NIST-traceable calibrated Ocean Optics HDX UV-Vis
141 spectroradiometer with an extreme solarization resistant 455 μ fiber and Spectralon

142 diffusing cosine corrector detector. Raw spectral data from the OceanView software
143 was interpolated to integer wavelengths using the FORECAST function in Microsoft
144 Excel and relativized to peak emission at 222 nm for use in dose calculations (Figures 1
145 and S1). Total incident UV-C irradiance was measured using an International Light
146 Technologies (ILT) 2400 radiometer with a SED 220/U solar blind detector, W Quartz
147 wide eye diffuser for cosine correction, and peak irradiance response NIST-traceable
148 calibration. For irradiance measurement, the peak wavelength calibration value was
149 input manually as the radiometer factor. The incident irradiance was measured with the
150 detection plane of the radiometer centered at the height and location of the sample
151 surface during UV exposures, and corrected for several factors to determine the
152 average irradiance through the sample depth. Spatial nonuniformity of emission was
153 accounted for each test by measuring irradiance at 0.5 cm increments from the center
154 to the edge of the petri dish and relativized to determine a petri factor, which was
155 always > 0.9. The typical detector spectral response was obtained from ILT and used to
156 calculate the radiometer factor integrated over the lamp emission, which was 0.9971.
157 As previously³⁴, the reflection factor for water at the 222 nm peak wavelength was
158 assumed to be 0.9726. The divergence factor was determined each experiment day by
159 accounting for the distance between the lamp and the sample surface, and the sample
160 depth and was always > 0.9. The water factor was determined each sample day by the
161 ratio between the incident irradiance and the average irradiance integrated through the
162 sample depth after wavelength-specific absorption. The UV-vis absorbance of virus
163 working stocks (prepared fresh for each test) was measured in the biosafety cabinet
164 using a NanodropTM One^C spectrophotometer via the microvolume pedestal for
165 wavelengths 200 - 295 nm and the 1 cm quartz cuvette for wavelengths above 195 nm.
166 Working stock absorbance spectra for each test are shown in Figures 1 and S1. After
167 these adjustments to incident irradiance in the center of the sample, the average
168 irradiance was used to calculate exposure times (max: 15 minutes; min: 15 seconds) for
169 pre-determined UV doses (0-40 mJ/cm²) (summarized in Supplementary Table S1).



170

171
172 **Figure 1:** (A) The raw spectral emission from 200 - 300 nm of the filtered KrCl excilamp
173 (USHIO Care222[®]) was interpolated and relativized to the peak emission at 222 nm for
174 use in UV dose calculations. (B) The absorbance spectrum from 200 - 300 nm of SARS-
175 CoV-2 at $\sim 10^5$ PFU/mL in cDMEM was measured for each of three biologically
176 independent Tests for use in UV dose calculations. Expanded emission and
177 absorbance spectra from 200 - 800 nm are shown in Supplementary Figure S1.

178 UV Treatment

179 All UV measurements, sample preparation, UV treatments, and subsequent handling of
180 treated samples were performed in a biosafety cabinet. On the day of each three
181 biologically independent tests while the UV source warmed up and measurements were
182 taken for dose calculations, aliquots of SARS-CoV-2 (previously tittered at 10^7 PFU/mL)
183 were diluted in cDMEM to make a “working stock solution” with a target titer of 10^5
184 PFU/mL. For each UV dose tested, 3 mL of the working stock solution was pipetted into

185 a 3.7 cm² area and 3.5 cm diameter polystyrene tissue culture dish (VWR Catalog #
186 82050-538) with a sterile Teflon-coated micro stir bar (VWR Catalog # 58948-353) and
187 positioned under the UV light on a small stir plate to achieve quiescent mixing while
188 blocking the UV light with a shutter. After removing the tissue culture dish lid, the
189 shutter was removed to expose the sample to UV light for the calculated exposure time
190 corresponding to the pre-determined UV dose before replacing the aperture to end the
191 UV exposure. Immediately afterwards, the treated media was transferred to a sterile 15
192 mL polypropylene centrifuge tube (VWR) and used for the assays described below.
193 Working stocks for untreated samples were placed on the stir plate for a representative
194 amount of time with the lamp off before transfer to centrifuge tube (0 mJ/cm²).

195 **SARS-CoV-2 plaque assay**

196 Plaque assays were used to determine PFU/mL of samples before UV treatment (0
197 mJ/cm²) and after UV treatment (all other UV doses). The plaque assay used for this
198 study is a modification of that which was originally developed and reported by Case et
199 al,³¹ and is listed here as STEPS 1-5. **(STEP 1)** At least 18 hours prior to the assay, 12-
200 well plates were seeded with a sufficient number of Vero cells so that each well was
201 confluent by the assay start; plates were incubated overnight at 37°C. **(STEP 2)** On the
202 day of the assay, serial dilutions of virus-containing media (e.g UV treated virus
203 samples) were prepared in cDMEM (1:10¹, 1:10², 1:10³, 1:10⁴) and warmed to 37°C.
204 **(STEP 3)** Media from each well of the 12-well plate was gently removed via pipette and
205 replaced with 500uL of each virus serial dilution, the volume pipetted down the side of
206 the well so as not to disturb the Vero cell monolayer. **(STEP 4)** The plate was incubated
207 for one hour at 37°C, 5% CO₂. **(STEP 5)** During that infection incubation period, a
208 solution comprising a 1:0.7 mixture of cDMEM and 2% methylcellulose (viscosity: 4000
209 cP) was freshly made and warmed to 37°C in a water bath. After the one hour infection
210 incubation period, the supernatant was removed from each well and replaced with 1 mL
211 of the warmed cDMEM/methylcellulose mixture. **(STEP 6)** The culture plate was then
212 returned to the incubator and left undisturbed for 3 days. On the final day,
213 cDMEM/methylcellulose mixture was removed from each well, cells were fixed with 4%
214 para-formaldehyde in PBS (20 minutes, room temperature), washed with PBS and

215 stained with 0.05% crystal violet (in 20% methanol). After rinsing plates with distilled
216 water, plates were dried and plaques were counted under a light microscope at 20X
217 magnification.

218 **SARS-CoV-2 outgrowth assay**

219 The virus outgrowth assay used for this study is identical to the plaque assay described
220 above, with the exception that after **STEP 4** the virus laden media was replaced with 1
221 mL of warm cDMEM (instead of a cDMEM/methylcellulose mixture). Afterwards, the
222 culture plate was returned to the incubator and left undisturbed for 3 days. On the final
223 day, the cell supernatants of each well were collected, transferred into a microcentrifuge
224 tube, centrifuged at low speed to remove cell debris (1,000 x *g*, 10 min), aliquoted into
225 microcentrifuge tubes, frozen and stored at -80°C. Aliquots were subsequently used for
226 quantitative real time PCR (qRT-PCR) measurement of SARS-CoV-2 nucleocapsid (N)
227 gene copies, as well as ELISA determination of SARS-CoV-2 N protein concentrations.

228 **SARS-CoV-2 N gene quantitation - N1 primer set**

229 Quantitative PCR (qPCR) was used to quantify the SARS-CoV-2 N gene directly in RNA
230 extracts of samples before UV treatment (0 mJ/cm²) and after UV treatment (all other
231 UV doses), and in RNA extracts of cell supernatant aliquots from outgrowth assays.
232 RNA was extracted from samples using the QIAamp Viral RNA method (Qiagen), and
233 converted to cDNA using the SuperScript IV first strand synthesis method with random
234 hexamer primers (Invitrogen). cDNA was subsequently amplified with the “N1 primer
235 set” and associated PCR conditions that were originally developed by the Centers for
236 Disease Control³⁵. These primers are specific to nucleotides 13-85 of the N gene (NCBI
237 Ref Seq NC_045512.2) and generate a short (72 nt) amplicon: 2019-nCoV_N1-F
238 (forward) primer, 5'-GACCCCAAATCAGCGAAAT-3'; 2019-nCoV_N1-R (reverse)
239 primer, 5'-TCTGGTTACTGCCAGTTGAATCTG-3'. cDNA was PCR-amplified in a
240 quantitative PCR (q-PCR) assay comprising 1X TaqMan Universal PCR Master Mix
241 (Applied Biosystems), the N1 forward/reverse primers described above (final
242 concentration: 500 nM) and a fluorophore-conjugated N1 TaqMan probe (5'-FAM-

243 ACCCCGCATTACGTTTGGTGGACC-BHQ1-3'; final concentration 125 nM). q-PCR
244 assays were run on a BioRad CFX Connect Real Time PCR system to determine C_T
245 values from samples and standards. A standard curve was generated for the N1 primer
246 set by running serial dilutions on each plate of *in vitro* transcribed RNA converted to
247 cDNA relating N gene copy numbers to C_T values. To generate this standard, RNA was
248 extracted from an aliquot of our SARS-CoV-2 stock and converted to cDNA before
249 amplification of the N gene using the N1 primer set as described above. The amplicon
250 was visualized by agarose gel electrophoresis, gel extracted and cloned/ligated into the
251 plasmid vector pCR II-TOPO (Invitrogen), downstream of the T7 promoter. Ligation
252 products were transformed into *E. coli*, and mini-preps of randomly selected colonies
253 were screened via PCR for the presence of insert. A single clone was then used to
254 produce *in vitro* transcribed (IVT) N gene RNA—a reagent necessary for accurate gene
255 copy number measurement—using the HiScribe T7 Quick High Yield RNA Synthesis
256 method (New England Biolabs). After treating the IVT RNA with DNase and performing
257 a cleanup reaction, the RNA concentration was determined via Nanodrop. The copies of
258 single stranded N gene RNA transcripts per μL was determined by the following
259 equation: [RNA concentration (Nanodrop measurement, $\text{ng}/\mu\text{L}$) x the Avogadro number
260 (6.02×10^{23})] / [Predicted molecular weight of transcript (23 kDa) x 10^9]. Serial dilutions
261 of IVT RNA were made (range: $10^{13} \rightarrow 10^{-1}$ copies/ μL), converted to cDNA as above and
262 used as standards in the N gene copy number assay described above.

263 **SARS-CoV-2 N gene quantitation - N1-2 primer set**

264 qPCR was used to quantify the SARS-CoV-2 N gene in RNA extracts of samples of
265 working stocks before UV treatment ($0 \text{ mJ}/\text{cm}^2$) and immediately after UV treatment (all
266 other UV doses). RNA was extracted from samples and converted to cDNA as
267 described above. cDNA was subsequently quantified using a combination of the CDC
268 2019 N1 and N2 primer sets to generate a long (944 nt) amplicon: 2019-nCoV_N1-F
269 (forward) primer, 5'-GACCCCAAATCAGCGAAAT-3'; 2019-nCoV_N2-R (reverse)
270 primer, 5'-GCGCGACATTCCGAAGAA-3'. Primers were obtained from IDT and final
271 concentrations were 500 nM, in 10 μL SsoFast EvaGreen Supermix (BIO-RAD) and
272 7.75 μL nuclease free water (Fisher Scientific) and 2 μL cDNA template. Reactions with

273 total volume of 20 μ L were run in at least technical duplicate on an Applied Biosystems
274 QuantStudio 7 Real-Time PCR system to determine C_T values from samples and
275 standards. For the N1-2 primer set, the standard consisted of serial dilutions of the
276 double stranded DNA control plasmid of the complete N gene (2019-nCoV_N_Positive
277 Control, IDT).

278

279 **SARS-CoV-2 N protein ELISA**

280 The concentration of N protein in outgrowth assay supernatants was determined using
281 the SARS-CoV-2 Antigen Quantitative Assay Kit (ELISA) method (ADS Biotec).
282 Manufacturer-provided calibration controls were used to establish a standard curve
283 related N protein concentration to sample absorbance (wavelength: 450 nm). Values
284 outside the standard curve were diluted further and rerun as appropriate. The positive
285 signal for SARS-CoV-2 was $2.7 \times 10^5 \pm 9.8 \times 10^4$ pg/mL in untreated virus samples at
286 Day 0 and $1.4 \times 10^8 \pm 3.0 \times 10^8$ pg/mL in cell culture supernatants incubated with
287 untreated virus samples at Day 3. No N protein was detected in negative control cell
288 culture supernatants that were incubated without virus samples.

289 **Graphing and Statistics**

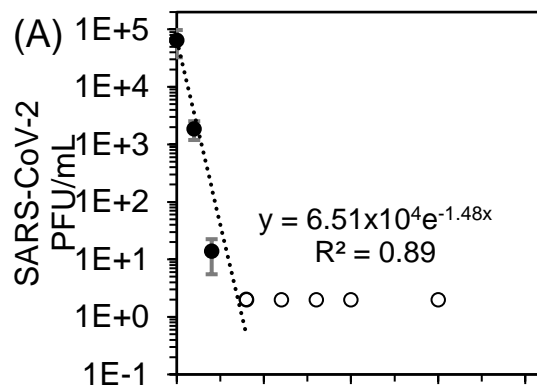
290 Graphs were prepared using either GraphPad Prism or Microsoft Excel programs;
291 statistical analyses (including regression using the data analysis add-in to determine
292 standard error of regression coefficients) were performed using these programs'
293 bundled software. \log_{10} Reduction (LR) was calculated as $\log_{10}(N_0/N)$, where N was
294 viral PFU/mL in the plaque assay, N gene copies/ μ L in qPCR assays for either the short
295 N1 amplicon or the long N1-2 amplicon, or N protein concentration in pg//mL in the
296 ELISA assay after exposure to a given UV₂₂₂ dose, and N_0 was the initial concentration.
297 The level of replication in this study was three biologically independent tests, with at
298 least technical duplicates for each assay.

299 **RESULTS**

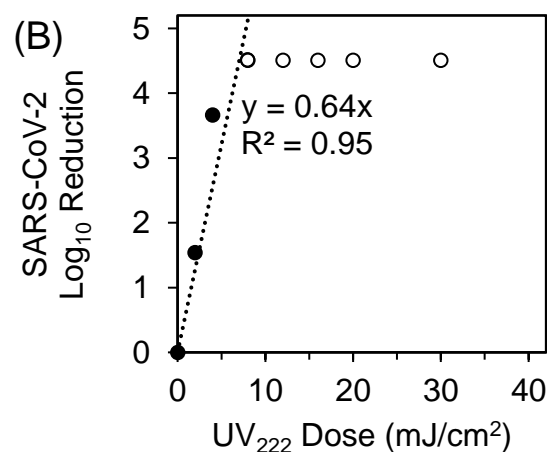
300 **SARS-CoV-2 Infectivity Response to UV₂₂₂**

301 Viral infectivity UV₂₂₂ dose response was characterized by exponential decay kinetics
302 (Figure 2). At a mean initial viral titer of 6.51×10^4 PFU/mL, the pseudo first order rate
303 constant for viral disinfection was $-1.48 \text{ cm}^2/\text{mJ}$ ($R^2 = 0.89$). When expressed as LR of
304 viral infectivity after exposure to a given UV dose, the linear rate constant was 0.64
305 cm^2/mJ ($R^2 = 0.95$), which equates to a D_{90} (dose for 1 log₁₀ or 90% inactivation) = 1.6
306 mJ/cm^2 . Doses ranges and initial Vero cell confluence were only sufficient in the Test 3
307 experimental replicate to quantify a dose response. However, in Test 2, the mean initial
308 viral titer of 3.54×10^4 PFU/mL in untreated samples was reduced to below detection by
309 the first dose tested of $10 \text{ mJ}/\text{cm}^2$, equivalent to a LR of at least 4.25 logs. These
310 results were also consistent with qualitative results from Test 1, where Vero cells
311 appeared mostly dead in the untreated samples, appeared increasingly healthy through
312 doses 0.7 and $1.4 \text{ mJ}/\text{cm}^2$, and appeared healthy at doses above $2 \text{ mJ}/\text{cm}^2$.
313

314



315



316

317 **Figure 2:** (A) SARS-CoV-2 titers measured by plaque assay 3 days after sample
318 exposure to each UV₂₂₂ dose (dark circles) were fit with an exponential model starting at
319 the mean initial (0 mJ/cm²) viral titer of 6.51x10⁴ PFU/mL through responses up to and
320 including 8 mJ/cm² where PFU/mL first dropped below the assay detection limit (DL) of
321 2 PFU/mL (hollow circles). Error bars represent standard deviation of at least two
322 technical replicates. (B) SARS-CoV-2 log₁₀ reductions (LR) of viral titers after exposure
323 to each UV₂₂₂ dose (dark circles) were fit with a linear model forced through the origin at
324 0 mJ/cm² through responses up to and including 8 mJ/cm² where LR first exceeded the
325 DL of 4.51 logs (hollow circles).

326 SARS-CoV-2 N Gene and Protein Response to UV₂₂₂

327 For the short amplicon spanning the N1 region of the N gene (CDC 2019), viral RNA
328 damage in response to UV₂₂₂ immediately after treatment was also characterized by

329 exponential decay kinetics (Figure 3A). When expressed as LR of N1 copies/ μ L in
330 qPCR reactions after exposure to a given UV dose, the linear rate constant was $0.069 \pm$
331 $0.005 \text{ cm}^2/\text{mJ}$ (slope \pm standard error, $R^2 = 0.92$). The N1 dose response was modeled
332 using the linear region between 0 - 20 mJ/cm^2 to avoid tailing in the dose response.
333 When including only doses up to $10\text{mJ}/\text{cm}^2$ as for the plaque assay, the slope and R^2 of
334 the N1 gene damage dose response was the same as for doses up to $20 \text{ mJ}/\text{cm}^2$.
335 Compared with the LR rate constant for of SARS-CoV-2 infectivity measured by plaque
336 assay, the LR rate constant of N gene damage measured by N1 qPCR was
337 approximately 10-fold lower. Across all tests, the positive signal for SARS-CoV-2 in the
338 N1 assay was $10.75 \pm 0.25 \log_{10}$ copies/ μ L in cell cultures infected with untreated virus
339 ($0 \text{ mJ}/\text{cm}^2$), $4.89 \pm 0.86 \log_{10}$ copies/ μ L in uninfected cell culture supernatants, 5.49
340 \log_{10} copies/ μ L in RNA extraction negative control, $3.36 \pm 0.24 \log_{10}$ copies/ μ L in no
341 template RT-qPCR reaction controls (concentration data and standard curves shown in
342 Supplementary Figures S2 and S3). Despite this background signal, dose responses
343 were still discernable. For the N1 dose response after 3 days in the outgrowth assay for
344 doses up to 0 - 20 mJ/cm^2 , the linear rate constant was $0.260 \pm 0.036 \text{ cm}^2/\text{mJ}$ (slope \pm
345 standard error, $R^2 = 0.76$). Although a positive dose response was apparent and the
346 slope was closer to the plaque assay (indicating better ability to predict plaque assay
347 dose response with combined cell culture with qPCR), the increased variability
348 introduced by cell culture decreased the strength of the regression.
349
350 For the long amplicon spanning both the N1 and N2 regions of N gene (CDC 2019),
351 viral RNA damage in response to UV_{222} immediately after treatment was also
352 characterized by exponential decay (Figure 3B). The linear rate constant for LR versus
353 UV_{222} dose was $0.054 \pm 0.003 \text{ cm}^2/\text{mJ}$ (slope \pm standard error, $R^2 = 0.94$). Compared
354 with the LR rate constant for of SARS-CoV-2 infectivity measured by plaque assay, the
355 LR rate constant of N gene damage measured by N1-2 qPCR was approximately 10-
356 fold lower. This similarity indicates that increasing the amplicon length did not increase
357 the ability to detect gene damage that correlates with loss of viral infectivity. Across all
358 tests, the positive signal for SARS-CoV-2 in the N1-2 assay was $4.6 \pm 0.1 \log_{10}$
359 copies/ μ L in cell cultures infected with untreated virus, undetected in uninfected cell

360 culture supernatants, and 0.8 ± 1.4 copies/ μ L in no template RT-qPCR reaction controls
361 (concentration data and standard curves shown in Supplementary Figures S2 and S3).
362 Because the long amplicon assay was used to investigate potential for improved
363 measurement of disinfection dose response without culture, no Day 3 samples were
364 analyzed.

365
366 Although no dose response was observed for LR of the N protein versus UV₂₂₂ dose
367 immediately after treatment for doses up to 40 mJ/cm² (0.002 ± 0.001 cm²/mJ, slope \pm
368 standard error, $R^2 = 0.21$), a stronger dose response was observed in Day 3 cell culture
369 supernatants for doses up to 20 mJ/cm² (0.243 ± 0.028 cm²/mJ, slope \pm standard error,
370 $R^2 = 0.21$) (Figure 3C). Across all tests, the positive signal for SARS-CoV-2 in the N
371 protein assay was $2.69 \times 10^5 \pm 9.83 \times 10^4$ pg/mL in untreated virus samples on Day 0,
372 $1.41 \times 10^8 \pm 2.99 \times 10^8$ in Day 3 cell culture supernatants infected with untreated virus,
373 and below detection in uninfected cell culture supernatants (concentration data and
374 standard curves shown in Supplementary Figures S2 and S3). Gene copies/ μ L for both
375 qPCR assays and protein pg/mL for the ELISA assay are shown for each UV₂₂₂ dose in
376 Supplementary Figure S2 and standard curves for all assays are shown in
377 Supplementary Figure S3.

378

379

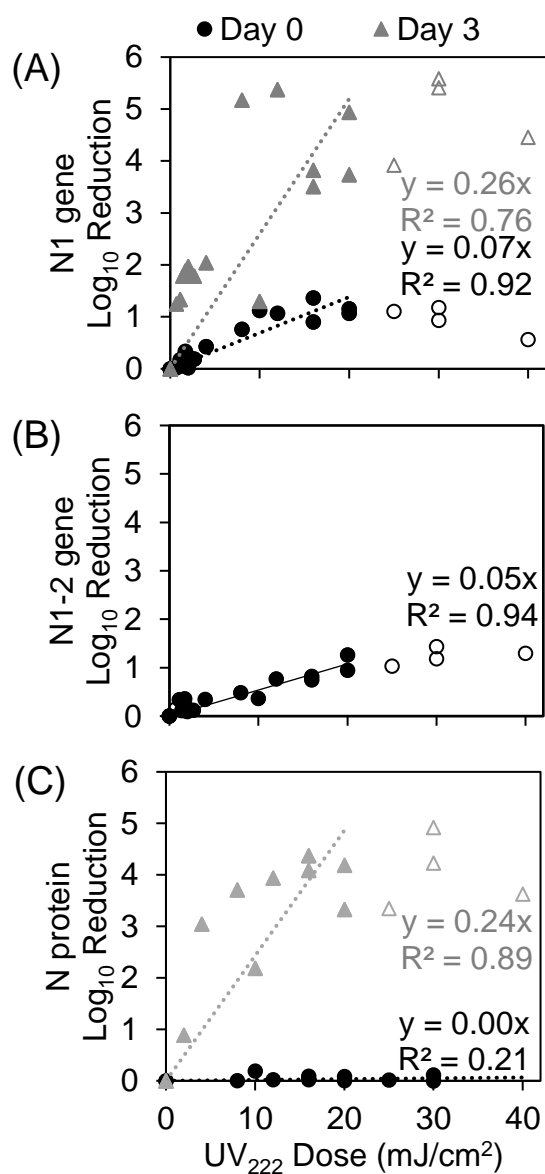
380

381

382

383

384 **Figure 3:** (A) SARS-CoV-2 N gene damage immediately after UV treatment (Day 0) and
385 after incubation of samples with host cells (Day 3) expressed as \log_{10} reduction of N1
386 (short amplicon) copies/ μL in qPCR reactions. (B) SARS-CoV-2 N gene damage
387 immediately after UV treatment (Day 0) expressed as \log_{10} reduction of N1-2 (long
388 amplicon) copies/ μL in qPCR reactions. (C) SARS-CoV-2 N protein concentration
389 measured by ELISA expressed as \log_{10} reduction of N protein concentration (pg/mL) in
390 samples immediately after UV treatment (Day 0) and after incubation of samples with
391 host cells (Day 3). SARS-CoV-2 \log_{10} reductions of the N1 amplicon, N1-2 amplicon, or



392 N protein versus UV₂₂₂ dose were fit with a linear model forced through the origin at 0
393 mJ/cm² through responses up to and including 20 mJ/cm² indicated by filled circles.
394 Points not included in models are indicated by hollow circles.

395

396 **DISCUSSION**

397 This study provides the first rigorous UV₂₂₂ dose response kinetics for SARS-CoV-2 in
398 aqueous solution, but there are limitations that must be acknowledged. Most
399 importantly, this study was conducted using virions suspended in aqueous solution.
400 This is only a starting point for quantifying dose response kinetics for airborne virus
401 disinfection that is most relevant for this virus, where many factors such as temperature,
402 humidity, air flow dynamics, and UV reactor specifics will impact dose responses.
403 Previous studies comparing disinfection kinetics of infectious agents in air at increasing
404 relative humidity to those in water^{36–41} indicate that these water dose responses may
405 present a conservative estimate of airborne disinfection kinetics because humidity in
406 many indoor environments is conditioned to reduce infectious agent persistence

407

408 One additional limitation of this study related to UV₂₂₂ application in indoor environments
409 is that the disinfection impact of any ozone production by vacuum UV wavelengths
410 potentially emitted by the KrCl excilamp was not measured, but can likely be neglected
411 due to high airflows in the biosafety cabinet and BSL3 facility. The negative air quality
412 impacts and building material degradation by ozone potentially generated by these
413 lamps, and the potential health hazards and building material solarization from
414 wavelengths below 240 nm and the nonzero emission at wavelengths above 240 nm
415 (Supplementary Figure S1), should also be considered when weighing the benefits of
416 reducing infectious disease transmission by UV₂₂₂ for COVID-19 and other infectious
417 diseases.

418

419 Considering these limitations, these data provide a strong foundation for future
420 development and application of UV₂₂₂ for reducing airborne viral transmission. UV₂₂₂ is
421 both 4.2 times safer for human exposure (the threshold limit values for human UV

422 exposure are 25 mJ/cm² and 6 mJ/cm² at 222 and 254 nm, respectively⁴¹) and at least
423 1.3 times as effective at disinfecting SARS-CoV-2 (the D₉₀ we observed for UV₂₂₂ (1.6
424 mJ/cm²) is lower than recently predicted by genomic modeling for UV₂₅₄ (2.15
425 mJ/cm²)⁴²). A recent study applying continuous UV₂₂₂ at doses below these threshold
426 limit values to treat other airborne coronaviruses demonstrated multiple logs of
427 inactivation within minutes⁴³. This low wavelength advantage for SARS-CoV-2
428 disinfection is consistent with a study where UV₂₂₂ was more than twice as effective as
429 UV₂₅₄ against MS2 bacteriophage³⁴ and with other viral action spectra indicating greater
430 sensitivity at 222 nm than 254 nm²⁶. A recent review⁴⁴ predicted the median D₉₀ for
431 coronavirus disinfection by UV₂₅₄ to be 3.7 mJ/cm². Our results and these predictions
432 are in general agreement with recent UV₂₂₂ and UV₂₅₄ disinfection studies of SARS-
433 CoV-2 as recently reviewed⁴¹. However, some of these studies are still in the process
434 of peer review and/or did not use standardized UV disinfection procedures that allow
435 comparisons between experiments and precise quantification of doses. In the only
436 UV₂₂₂ SARS-CoV-2 surface decontamination study to date ⁴⁵, researchers report 0.94
437 LR after 10 second exposure to 0.1 mW/cm². Although UV dose cannot be calculated
438 for this study in the absence of sample absorbance and differences in experimental
439 setup, these results demonstrate a high degree of susceptibility of SARS-CoV-2 to
440 UV₂₂₂ and generally align with ours.

441
442 Considering our data in context of literature, UV₂₂₂ is a promising disinfection method for
443 SARS-CoV-2 in aqueous solution. These infectivity and molecular dose response data
444 could immediately inform measures to prevent transmission by water or wastewater
445 where infectious SARS-CoV-2 and other viruses have been shown to be potentially
446 persistent for days^{46,47}. Although tailing was observed in dose responses for molecular
447 assays and may have been contributed from clumping of virus in the protein-laden
448 growth media, viruses were disinfected below detection in plaque assays, indicating that
449 aggregation did not interfere with complete viral inactivation. We did not observe a
450 strong relationship between the kinetics of N gene damage (measured by qPCR with a
451 short and long amplicon) and disinfection, which could reflect that protein damage
452 contributes more to disinfection than genome damage for SARS-CoV-2. One study of

453 MS2 bacteriophage found RNA genome damage to be closely related to and thus
454 contributed to disinfection kinetics²⁷, whereas a study of Adenovirus found DNA genome
455 damage not to be closely related to disinfection⁴⁸. This disparity between these viruses
456 with different structures and hosts was further demonstrated when it was shown that
457 protein damage, especially to external capsid proteins, contributes more strongly to UV
458 disinfection of Adenovirus⁴⁹. However, we also did not see a strong association
459 between the kinetics of N protein damage and disinfection. Because we only measured
460 the N protein that closely associates with the viral genome, we may have missed
461 damage to external proteins such as the spike protein which are on the surface to
462 absorb incoming UV radiation and are vital in infection of host cells⁵⁰. Additionally, the
463 confirmation and sequence of the genome and proteins can affect UV genetic
464 damage⁵¹⁻⁵⁵, so the N protein and gene may not be the targets that primarily contribute
465 to disinfection-inducing molecular damage. These factors could explain the weak
466 relationships we observed between disinfection kinetics and N gene damage or N
467 protein damage, and warrant further investigation to unravel the mechanisms of
468 disinfection at this and other UV wavelengths. While these mechanistic complexities
469 remain to be resolved, the disinfection kinetics we report indicate the high degree of
470 susceptibility of SARS-CoV-2 in aqueous solution to UV₂₂₂.

471

472 **ACKNOWLEDGEMENTS**

473 This work was supported by funds from The Ohio State University (OSU) Sustainability
474 Institute; OSU Infectious Disease Institute; OSU Department of Civil, Environmental,
475 and Geodetic Engineering (Chair: Dr. Allison MacKay); OSU Department of Microbial
476 Infection & Immunity (Chair: Dr. Eugene Oltz); and National Institutes of Health (U54
477 CA260582). Anna Herman of AquiSense Technologies shared a list of references to
478 SARS-CoV-2 UV disinfection studies. The UV₂₂₂ light source (USHIO Care222®) was
479 provided by USHIO, Inc. through material transfer agreement 2020-2654 to Hull at
480 OSU.

481

482 REFERENCES

- 483 (1) Samet, J. M.; Prather, K.; Benjamin, G.; Lakdawala, S.; Lowe, J.-M.; Reingold, A.;
484 Volckens, J.; Marr, L. Airborne Transmission of SARS-CoV-2: What We Know.
485 *Clin. Infect. Dis.* **2021**. <https://doi.org/10.1093/cid/ciab039>.
- 486 (2) Tang, J. W.; Bahnfleth, W. P.; Bluysen, P. M.; Buonanno, G.; Jimenez, J. L.;
487 Kurnitski, J.; Li, Y.; Miller, S.; Sekhar, C.; Morawska, L.; et al. Dismantling Myths
488 on the Airborne Transmission of Severe Acute Respiratory Syndrome
489 Coronavirus (SARS-CoV-2). *J. Hosp. Infect.* **2021**.
490 <https://doi.org/10.1016/j.jhin.2020.12.022>.
- 491 (3) Hess, C. B.; Buchwald, Z. S.; Stokes, W.; Nasti, T. H.; Switchenko, J. M.;
492 Weinberg, B. D.; Steinberg, J. P.; Godette, K. D.; Murphy, D.; Ahmed, R.; et al.
493 Low-Dose Whole-Lung Radiation for COVID-19 Pneumonia: Planned Day 7
494 Interim Analysis of a Registered Clinical Trial. *Cancer* **2020**, *126* (23), 5109–5113.
495 <https://doi.org/10.1002/cncr.33130>.
- 496 (4) Wang, Y.; Zhang, D.; Du, G.; Du, R.; Zhao, J.; Jin, Y.; Fu, S.; Gao, L.; Cheng, Z.;
497 Lu, Q.; et al. Remdesivir in Adults with Severe COVID-19: A Randomised,
498 Double-Blind, Placebo-Controlled, Multicentre Trial. *Lancet* **2020**, *395* (10236),
499 1569–1578. [https://doi.org/10.1016/S0140-6736\(20\)31022-9](https://doi.org/10.1016/S0140-6736(20)31022-9).
- 500 (5) Ison, M. G.; Scheetz, M. H. Understanding the Pharmacokinetics of Favipiravir:
501 Implications for Treatment of Influenza and COVID-19. *EBioMedicine*. Elsevier
502 B.V. January 1, 2021. <https://doi.org/10.1016/j.ebiom.2020.103204>.
- 503 (6) Cavalcanti, A. B.; Zampieri, F. G.; Rosa, R. G.; Azevedo, L. C. P.; Veiga, V. C.;
504 Avezum, A.; Damiani, L. P.; Marcadenti, A.; Kawano-Dourado, L.; Lisboa, T.; et
505 al. Hydroxychloroquine with or without Azithromycin in Mild-to-Moderate Covid-19.
506 *N. Engl. J. Med.* **2020**, *383* (21), 2041–2052.
507 <https://doi.org/10.1056/nejmoa2019014>.
- 508 (7) Monk, P. D.; Marsden, R. J.; Tear, V. J.; Brookes, J.; Batten, T. N.; Mankowski,
509 M.; Gabbay, F. J.; Davies, D. E.; Holgate, S. T.; Ho, L. P.; et al. Safety and
510 Efficacy of Inhaled Nebulised Interferon Beta-1a (SNG001) for Treatment of
511 SARS-CoV-2 Infection: A Randomised, Double-Blind, Placebo-Controlled, Phase

- 512 2 Trial. *Lancet Respir. Med.* **2020**. [https://doi.org/10.1016/S2213-2600\(20\)30511-](https://doi.org/10.1016/S2213-2600(20)30511-)
513 7.
- 514 (8) Simonovich, V. A.; Burgos Pratx, L. D.; Scibona, P.; Beruto, M. V.; Vallone, M. G.;
515 Vázquez, C.; Savoy, N.; Giunta, D. H.; Pérez, L. G.; Sánchez, M. del L.; et al. A
516 Randomized Trial of Convalescent Plasma in Covid-19 Severe Pneumonia. *N.*
517 *Engl. J. Med.* **2020**. <https://doi.org/10.1056/nejmoa2031304>.
- 518 (9) Joyner, M. J.; Carter, R. E.; Senefeld, J. W.; Klassen, S. A.; Mills, J. R.; Johnson,
519 P. W.; Theel, E. S.; Wiggins, C. C.; Bruno, K. A.; Klompas, A. M.; et al.
520 Convalescent Plasma Antibody Levels and the Risk of Death from Covid-19. *N.*
521 *Engl. J. Med.* **2021**. <https://doi.org/10.1056/nejmoa2031893>.
- 522 (10) Weinreich, D. M.; Sivapalasingam, S.; Norton, T.; Ali, S.; Gao, H.; Bhore, R.;
523 Musser, B. J.; Soo, Y.; Rofail, D.; Im, J.; et al. REGN-COV2, a Neutralizing
524 Antibody Cocktail, in Outpatients with Covid-19. *N. Engl. J. Med.* **2020**, *384* (3).
525 <https://doi.org/10.1056/nejmoa2035002>.
- 526 (11) Chen, P.; Nirula, A.; Heller, B.; Gottlieb, R. L.; Boscia, J.; Morris, J.; Huhn, G.;
527 Cardona, J.; Mocherla, B.; Stosor, V.; et al. SARS-CoV-2 Neutralizing Antibody
528 LY-CoV555 in Outpatients with Covid-19. *N. Engl. J. Med.* **2020**, *384* (3).
529 <https://doi.org/10.1056/nejmoa2029849>.
- 530 (12) Dexamethasone in Hospitalized Patients with Covid-19 — Preliminary Report. *N.*
531 *Engl. J. Med.* **2020**. <https://doi.org/10.1056/nejmoa2021436>.
- 532 (13) Stone, J. H.; Frigault, M. J.; Serling-Boyd, N. J.; Fernandes, A. D.; Harvey, L.;
533 Foulkes, A. S.; Horick, N. K.; Healy, B. C.; Shah, R.; Bensaci, A. M.; et al. Efficacy
534 of Tocilizumab in Patients Hospitalized with Covid-19. *N. Engl. J. Med.* **2020**, *383*
535 (24), 2333–2344. <https://doi.org/10.1056/nejmoa2028836>.
- 536 (14) Cao, Y.; Wei, J.; Zou, L.; Jiang, T.; Wang, G.; Chen, L.; Huang, L.; Meng, F.;
537 Huang, L.; Wang, N.; et al. Ruxolitinib in Treatment of Severe Coronavirus
538 Disease 2019 (COVID-19): A Multicenter, Single-Blind, Randomized Controlled
539 Trial. *J. Allergy Clin. Immunol.* **2020**, *146* (1), 137-146.e3.
540 <https://doi.org/10.1016/j.jaci.2020.05.019>.
- 541 (15) Polack, F. P.; Thomas, S. J.; Kitchin, N.; Absalon, J.; Gurtman, A.; Lockhart, S.;
542 Perez, J. L.; Pérez Marc, G.; Moreira, E. D.; Zerbini, C.; et al. Safety and Efficacy

- 543 of the BNT162b2 mRNA Covid-19 Vaccine. *N. Engl. J. Med.* **2020**, 383 (27),
544 2603–2615. <https://doi.org/10.1056/nejmoa2034577>.
- 545 (16) Goel, S.; Hawi, S.; Goel, G.; Thakur, V. K.; Agrawal, A.; Hoskins, C.; Pearce, O.;
546 Hussain, T.; Upadhyaya, H. M.; Cross, G.; et al. Resilient and Agile Engineering
547 Solutions to Address Societal Challenges Such as Coronavirus Pandemic. *Mater.*
548 *Today Chem.* **2020**, 17. <https://doi.org/10.1016/j.mtchem.2020.100300>.
- 549 (17) Gerchman, Y.; Mamane, H.; Friedman, N.; Mandelboim, M. UV-LED Disinfection
550 of Coronavirus: Wavelength Effect. *J. Photochem. Photobiol. B Biol.* **2020**, 212.
551 <https://doi.org/10.1016/j.jphotobiol.2020.112044>.
- 552 (18) Kariwa, H.; Fujii, N.; Takashima, I. Inactivation of SARS Coronavirus by Means of
553 Povidone-Iodine, Physical Conditions and Chemical Reagents. *Dermatology*
554 **2006**, 212 (SUPPL. 1), 119–123. <https://doi.org/10.1159/000089211>.
- 555 (19) Darnell, M. E. R.; Subbarao, K.; Feinstone, S. M.; Taylor, D. R. Inactivation of the
556 Coronavirus That Induces Severe Acute Respiratory Syndrome, SARS-CoV. *J.*
557 *Viol. Methods* **2004**, 121 (1), 85–91.
558 <https://doi.org/10.1016/j.jviromet.2004.06.006>.
- 559 (20) Rabenau, H. F.; Cinatl, J.; Morgenstern, B.; Bauer, G.; Preiser, W.; Doerr, H. W.
560 Stability and Inactivation of SARS Coronavirus. *Med. Microbiol. Immunol.* **2005**,
561 194 (1–2), 1–6. <https://doi.org/10.1007/s00430-004-0219-0>.
- 562 (21) Pfeifer, G. P.; Besaratinia, A. UV Wavelength-Dependent DNA Damage and
563 Human Non-Melanoma and Melanoma Skin Cancer. *Photochemical and*
564 *Photobiological Sciences*. Royal Society of Chemistry 2012, pp 90–97.
565 <https://doi.org/10.1039/c1pp05144j>.
- 566 (22) Jose, J. G.; Pitts, D. G. Wavelength Dependency of Cataracts in Albino Mice
567 Following Chronic Exposure. *Exp. Eye Res.* **1985**, 41 (4), 545–563.
568 [https://doi.org/10.1016/S0014-4835\(85\)80011-7](https://doi.org/10.1016/S0014-4835(85)80011-7).
- 569 (23) Bjørklund, G.; Dadar, M.; Mutter, J.; Aaseth, J. The Toxicology of Mercury:
570 Current Research and Emerging Trends. *Environmental Research*. Academic
571 Press Inc. 2017, pp 545–554. <https://doi.org/10.1016/j.envres.2017.08.051>.
- 572 (24) Buonanno, M.; Ponnaiya, B.; Welch, D.; Stanislauskas, M.; Randers-Pehrson, G.;
573 Smilenov, L.; Lowy, F. D.; Owens, D. M.; Brenner, D. J. Germicidal Efficacy and

- 574 Mammalian Skin Safety of 222-Nm UV Light. *Radiat. Res.* **2017**, *187* (4), 483–
575 491. <https://doi.org/10.1667/RR0010CC.1>.
- 576 (25) Kaidzu, S.; Sugihara, K.; Sasaki, M.; Nishiaki, A.; Igarashi, T.; Tanito, M.
577 Evaluation of Acute Corneal Damage Induced by 222-Nm and 254-Nm Ultraviolet
578 Light in Sprague–Dawley Rats. *Free Radic. Res.* **2019**, *53* (6), 611–617.
579 <https://doi.org/10.1080/10715762.2019.1603378>.
- 580 (26) Beck, S. E.; Wright, H. B.; Hargy, T. M.; Larason, T. C.; Linden, K. G. Action
581 Spectra for Validation of Pathogen Disinfection in Medium-Pressure Ultraviolet
582 (UV) Systems. *Water Res.* **2015**, *70*, 27–37.
583 <https://doi.org/10.1016/j.watres.2014.11.028>.
- 584 (27) Beck, S. E.; Rodriguez, R. A.; Hawkins, M. A.; Hargy, T. M.; Larason, T. C.;
585 Linden, K. G. Comparison of UV-Induced Inactivation and RNA Damage in MS2
586 Phage across the Germicidal UV Spectrum. *Appl. Environ. Microbiol.* **2016**, *82*
587 (5), 1468–1474. <https://doi.org/10.1128/AEM.02773-15>.
- 588 (28) Beck, S. E.; Hull, N. M.; Poepping, C.; Linden, K. G. Wavelength-Dependent
589 Damage to Adenoviral Proteins Across the Germicidal UV Spectrum. *Environ. Sci.*
590 *Technol.* **2018**. <https://doi.org/10.1021/acs.est.7b04602>.
- 591 (29) Eischeid, A. C.; Linden, K. G. Molecular Indications of Protein Damage in
592 Adenoviruses after UV Disinfection. *Appl. Environ. Microbiol.* **2011**, *77* (3), 1145–
593 1147. <https://doi.org/10.1128/AEM.00403-10>.
- 594 (30) Hull, N. M.; Linden, K. G. Synergy of MS2 Disinfection by Sequential Exposure to
595 Tailored UV Wavelengths. *Water Res.* **2018**.
596 <https://doi.org/10.1016/j.watres.2018.06.017>.
- 597 (31) Case, J. B.; Bailey, A. L.; Kim, A. S.; Chen, R. E.; Diamond, M. S. Growth,
598 Detection, Quantification, and Inactivation of SARS-CoV-2. *Virology* **2020**, *548*,
599 39–48. <https://doi.org/10.1016/j.virol.2020.05.015>.
- 600 (32) Bolton, J. R.; Linden, K. G. Standardization of Methods for Fluence (UV Dose)
601 Determination in Bench-Scale UV Experiments. *J. Environ. Eng.* **2003**, *129* (3),
602 209–215. [https://doi.org/10.1061/\(asce\)0733-9372\(2003\)129:3\(209\)](https://doi.org/10.1061/(asce)0733-9372(2003)129:3(209)).
- 603 (33) Linden, K. G.; Darby, J. L. Estimating Effective Germicidal Dose from Medium
604 Pressure UV Lamps. *J. Environ. Eng.* **1997**, *123* (11), 1142–1149.

- 605 [https://doi.org/10.1061/\(asce\)0733-9372\(1997\)123:11\(1142\)](https://doi.org/10.1061/(asce)0733-9372(1997)123:11(1142)).
- 606 (34) Hull, N. M.; Linden, K. G. Synergy of MS2 Disinfection by Sequential Exposure to
607 Tailored UV Wavelengths. *Water Res.* **2018**.
608 <https://doi.org/10.1016/j.watres.2018.06.017>.
- 609 (35) CDC. Real-time RT-PCR Primers and Probes for COVID-19 | CDC
610 <https://www.cdc.gov/coronavirus/2019-ncov/lab/rt-pcr-panel-primer-probes.html>
611 (accessed Feb 4, 2021).
- 612 (36) Peccia, J.; Hernandez, M. UV-Induced Inactivation Rates for Airborne
613 *Mycobacterium Bovis* BCG. *J. Occup. Environ. Hyg.* **2004**, *1* (7), 430–435.
614 <https://doi.org/10.1080/15459620490458495>.
- 615 (37) Walker, C. M.; Ko, G. Effect of Ultraviolet Germicidal Irradiation on Viral Aerosols.
616 *Environ. Sci. Technol.* **2007**, *41* (15), 5460–5465.
617 <https://doi.org/10.1021/es070056u>.
- 618 (38) Jordan, P.; Werth, H. M.; Shelly, M.; Mark, H. Effects of Relative Humidity on the
619 Ultraviolet Induced Inactivation of Airborne Bacteria. *Aerosol Sci. Technol.* **2001**,
620 *35* (3), 728–740. <https://doi.org/10.1080/02786820152546770>.
- 621 (39) Kowalski, W. *Ultraviolet Germicidal Irradiation Handbook: UVGI for Air and*
622 *Surface Disinfection*; Springer Berlin Heidelberg, 2009.
623 <https://doi.org/10.1007/978-3-642-01999-9>.
- 624 (40) Tseng, C.-C.; Li, C.-S. Inactivation of Virus-Containing Aerosols by Ultraviolet
625 Germicidal Irradiation. *Aerosol Sci. Technol.* **2005**, *39* (12), 1136–1142.
626 <https://doi.org/10.1080/02786820500428575>.
- 627 (41) Raeiszadeh, M.; Adeli, B. A Critical Review on Ultraviolet Disinfection Systems
628 against COVID-19 Outbreak: Applicability, Validation, and Safety Considerations.
629 **2020**. <https://doi.org/10.1021/acsp Photonics.0c01245>.
- 630 (42) Pendyala, B.; Patras, A.; Pokharel, B.; D’Souza, D. Genomic Modeling as an
631 Approach to Identify Surrogates for Use in Experimental Validation of SARS-CoV-
632 2 and HuNoV Inactivation by UV-C Treatment. *Front. Microbiol.* **2020**, *11*, 2406.
633 <https://doi.org/10.3389/fmicb.2020.572331>.
- 634 (43) Buonanno, M.; Welch, D.; Shuryak, I.; Brenner, D. J. Far-UVC Light (222 Nm)
635 Efficiently and Safely Inactivates Airborne Human Coronaviruses. *Sci. Rep.* **2020**,

- 636 10 (1). <https://doi.org/10.1038/s41598-020-67211-2>.
- 637 (44) Heßling, M.; Hönes, K.; Vatter, P.; Lingenfelder, C. Ultraviolet Irradiation Doses
638 for Coronavirus Inactivation - Review and Analysis of Coronavirus
639 Photoinactivation Studies. *GMS Hyg. Infect. Control* **2020**, *15*, Doc08.
640 <https://doi.org/10.3205/dgkh000343>.
- 641 (45) Kitagawa, H.; Nomura, T.; Nazmul, T.; Omori, K.; Shigemoto, N.; Sakaguchi, T.;
642 Ohge, H. Effectiveness of 222-Nm Ultraviolet Light on Disinfecting SARS-CoV-2
643 Surface Contamination. *Am. J. Infect. Control* **2020**, *0* (0).
644 <https://doi.org/10.1016/j.ajic.2020.08.022>.
- 645 (46) Bivins, A.; Greaves, J.; Fischer, R.; Yinda, K. C.; Ahmed, W.; Kitajima, M.;
646 Munster, V. J.; Bibby, K. Persistence of SARS-CoV-2 in Water and Wastewater.
647 *Environ. Sci. Technol. Lett.* **2020**, *7* (12), 937–942.
648 <https://doi.org/10.1021/acs.estlett.0c00730>.
- 649 (47) Ye, Y.; Ellenberg, R. M.; Graham, K. E.; Wigginton, K. R. Survivability,
650 Partitioning, and Recovery of Enveloped Viruses in Untreated Municipal
651 Wastewater. *Environ. Sci. Technol.* **2016**, *50* (10), 5077–5085.
652 <https://doi.org/10.1021/acs.est.6b00876>.
- 653 (48) Rodríguez, R. A.; Bounty, S.; Linden, K. G. Long-Range Quantitative PCR for
654 Determining Inactivation of Adenovirus 2 by Ultraviolet Light. *J. Appl. Microbiol.*
655 **2013**, *114* (6), 1854–1865. <https://doi.org/10.1111/jam.12169>.
- 656 (49) Beck, S. E.; Hull, N. M.; Poepping, C.; Linden, K. G. Wavelength-Dependent
657 Damage to Adenoviral Proteins Across the Germicidal UV Spectrum. *Environ. Sci.*
658 *Technol.* **2018**, *52* (1), 223–229. <https://doi.org/10.1021/acs.est.7b04602>.
- 659 (50) Shang, J.; Wan, Y.; Luo, C.; Ye, G.; Geng, Q.; Auerbach, A.; Li, F. Cell Entry
660 Mechanisms of SARS-CoV-2. *Proc. Natl. Acad. Sci. U. S. A.* **2020**, *117* (21).
661 <https://doi.org/10.1073/pnas.2003138117>.
- 662 (51) Rockey, N.; Young, S.; Kohn, T.; Pecson, B.; Wobus, C. E.; Raskin, L.; Wigginton,
663 K. R. UV Disinfection of Human Norovirus: Evaluating Infectivity Using a Genome-
664 Wide PCR-Based Approach. *Environ. Sci. Technol.* **2020**, *54* (5), 2851–2858.
665 <https://doi.org/10.1021/acs.est.9b05747>.
- 666 (52) Ye, Y.; Chang, P. H.; Hartert, J.; Wigginton, K. R. Reactivity of Enveloped Virus

- 667 Genome, Proteins, and Lipids with Free Chlorine and UV254. *Environ. Sci.*
668 *Technol.* **2018**, 52 (14), 7698–7708. <https://doi.org/10.1021/acs.est.8b00824>.
- 669 (53) Wigginton, K. R.; Menin, L.; Sigstam, T.; Gannon, G.; Cascella, M.; Hisham, J;
670 Hamidane, B.; Tsybin, Y. O.; Waridel, P.; Kohn, T. UV Radiation Induces
671 Genome-Mediated, Site-Specific Cleavage in Viral Proteins. *ChemBioChem* **2012**,
672 13, 837–845. <https://doi.org/10.1002/cbic.201100601>.
- 673 (54) Wigginton, K. R.; Kohn, T. Virus Disinfection Mechanisms: The Role of Virus
674 Composition, Structure, and Function. *Current Opinion in Virology*. Elsevier B.V.
675 February 1, 2012, pp 84–89. <https://doi.org/10.1016/j.coviro.2011.11.003>.
- 676 (55) Wigginton, K. R.; Pecson, B. M.; Sigstam, T.; Bosshard, F.; Kohn, T. Virus
677 Inactivation Mechanisms: Impact of Disinfectants on Virus Function and Structural
678 Integrity. *Environ. Sci. Technol.* **2012**, 46 (21), 12069–12078.
679 <https://doi.org/10.1021/es3029473>.
- 680
- 681

682 **SARS-CoV-2 disinfection in aqueous solution**
683 **by UV₂₂₂ from a krypton chlorine excilamp**
684
685

686 **AUTHORS**

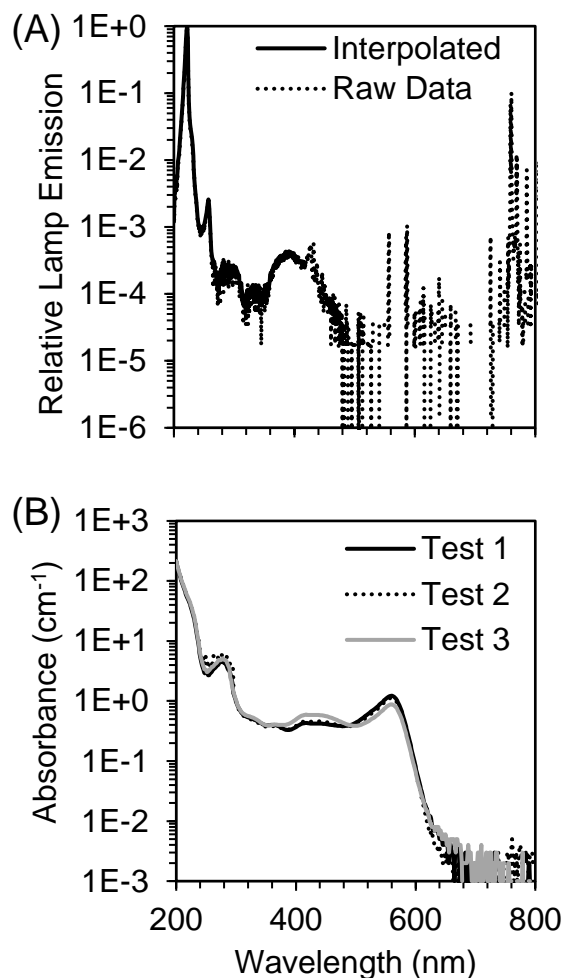
687 Richard T. Robinson^{1,2}, Najmus Mahfooz¹, Oscar Rosas-Mejia¹, Yijing Liu³, Natalie M.
688 Hull^{3,4*}
689

690 **AFFILIATIONS**

- 691 5. Department of Microbial Infection and Immunity, The Ohio State University,
692 Columbus, OH, USA
693 6. Infectious Diseases Institute, The Ohio State University, Columbus, OH, USA
694 7. Department of Civil, Environmental, and Geodetic Engineering, The Ohio State
695 University, Columbus, OH, USA
696 8. Sustainability Institute, The Ohio State University, Columbus, OH, USA
697 * Corresponding author: Natalie Hull, hull.305@osu.edu, 2070 Neil Ave, Hitchcock
698 417C, Columbus, OH,43210
699
700

701 **CONTENTS**

702 This supplementary information contains Figure S1 describing lamp emission and
703 sample absorbance, Table S1 describing key parameters for UV exposures and dose
704 calculations, Figure S2 standard curves for qPCR and ELISA assays, and Figure S3
705 molecular assay concentration data for N gene or N protein at each UV dose.
706
707



708

709

710 **Figure S1:** (A) The raw spectral emission from 200 - 300 nm of the filtered excilamp
711 (USHIO Care222[®]) was interpolated and relativized to the peak emission at 222 nm for
712 use in UV dose calculations and plotted on log scale to show orders of magnitude less
713 but non-zero emission at filtered wavelengths > 240 nm. (B) The absorbance spectrum
714 from 200 - 300 nm of SARS-CoV-2 at $\sim 10^5$ PFU/mL in cDMEM was measured for each
715 of three Tests for use in UV dose calculations.

716

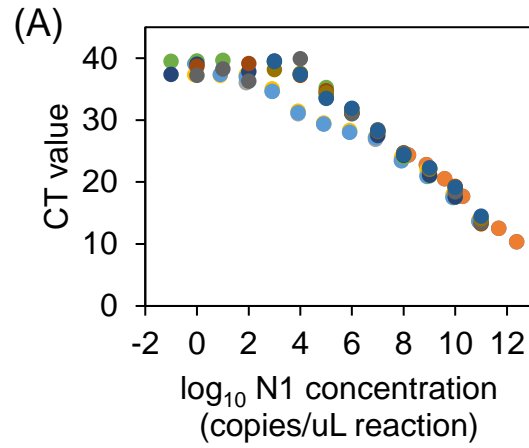
717

718 **Table S1:** Summary of key UV dose calculation parameters for each independent Test.

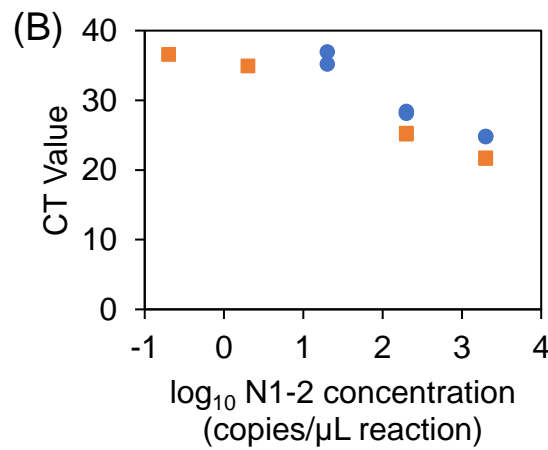
	Test 1	Test 2	Test 3
Date	1-Sep-20	16-Sep-20	4-Nov-20
UV doses (mJ/cm²)	0, 0.7, 1.1, 1.4, 1.7, 2.0, 2.7	0, 10, 16, 20, 25, 30, 40	0, 2, 4, 8, 12, 16, 20, 30
Sample exposure times (sec)	0, 29, 45, 57, 72, 87, 115	0, 214, 343, 429, 536, 643, 856	0, 84, 168, 336, 504, 672, 840, 1260
Incident irradiance at center of petri dish (mW/cm²)	1.100	2.490	1.200
Divergence factor	0.9444	0.9091	0.9091
Petri factor	0.9459	0.9147	0.9791
Water factor	0.0247	0.0232	0.0230
Average irradiance through sample depth (mW/cm²)	0.0236	0.0466	0.0238

719

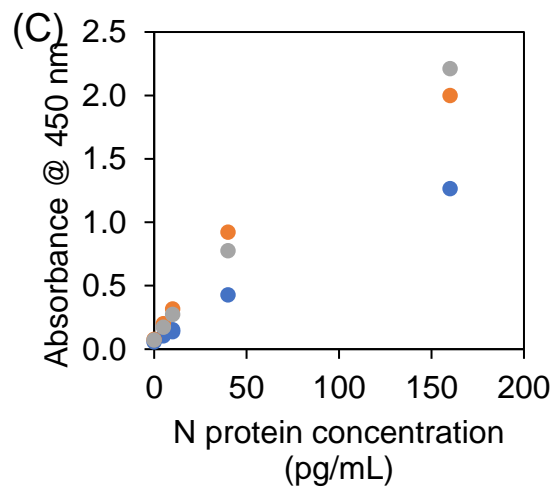
720



721



722

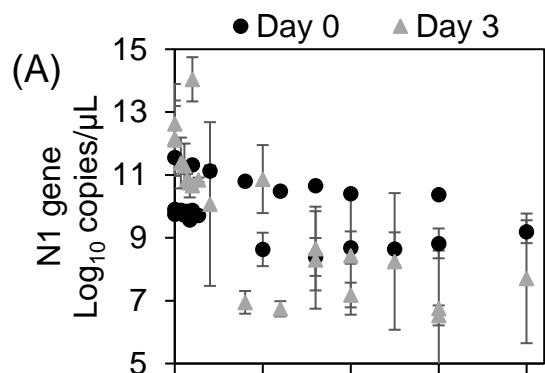


723

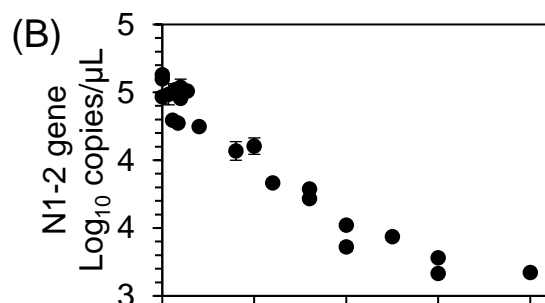
724 **Figure S2:** N gene RT-qPCR standard curves gene copies/ μ L reaction for the (A) short
725 N1 amplicon and (B) long N1-2 amplicon and (C) ELISA N protein standard curve.

726 Colors differentiate individual assay runs.

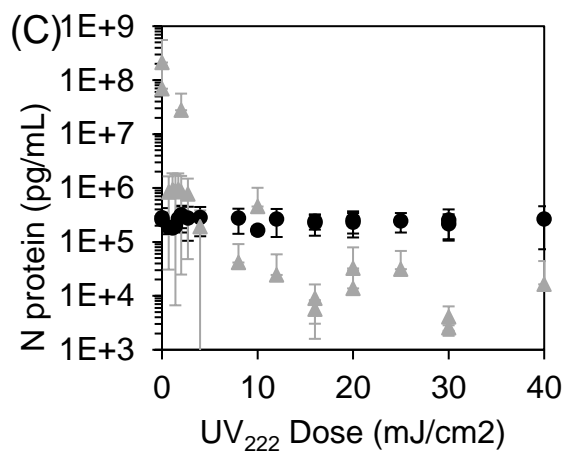
727



728



729



730

731 **Figure S3:** N gene RT-qPCR copies/μL reaction for the (A) short N1 amplicon and (B)
732 long N1-2 amplicon, where error bars represent standard deviation of at least two
733 technical replicates and could include technical replicates averaged across dilutions.
734 (C) N protein ELISA pg/mL, where error bars represent standard deviation of at least
735 two technical replicates and could include technical replicates averaged across
736 dilutions. Day 0 samples were analyzed immediately after UV irradiation, where Day 3
737 samples were analyzed in culture supernatants after incubation of samples with host
738 cells.